

Qualitative Research: The Impact of Root Orientation on Coarse Roots Detection Using Ground-Penetrating Radar (GPR)

Mingkai Wang,^{a,b} Jian Wen,^{a,b,*} and Wenbin Li^{a,b}

The growth of coarse roots is complex, leading to intricate patterns of root systems in three dimensions. To detect and recognize coarse roots, ground-penetrating radar (GPR) was used. According to the GPR theory, a clear profile hyperbola is formed on the GPR radargrams when electromagnetic waves travel across two surfaces with different dielectric constants. First, the forward models (different root orientations) were built with simulation software (GprMax3.0) based on the finite-difference time-domain method (FDTD). As the radar moved forward, the signal reflection curve was generated in different root orientations. An algorithm was proposed to obtain the coordinates of a single coarse root and analyze the influence of root direction on the hyperbola of coarse root through a symmetry curve and relative error (RE). Based on GPR datasets from the simulation experiment, the controlled experiment evaluated feasibility and effectiveness of the simulation experiment. To demonstrate the effect of the root orientation, the algorithm was applied to *in situ* recognition of the Summer Palace. The results showed that the localization of root orientation was relatively accurate. However, the proposed algorithm was unable to implement automatic detection, and the results still required human intervention. This research provides a solid basis for the biomass measurement, diameter estimation, and especially the three-dimensional reconstruction of ancient and famous trees.

Keywords: Coarse root systems; Root orientation; In situ recognition; Symmetry algorithm; Hough transform

Contact information: a: School of Technology, Beijing Forestry University, Beijing 100083, P. R. China; misslittlesheep@163.com; leewb@bjfu.edu.cn; b: Key Lab of State Forestry and Grassland Administration for Forestry Equipment and Automation, Beijing 100083, P. R. China;

* Corresponding author: wenjian@bjfu.edu.cn

INTRODUCTION

Coarse roots (> 2 mm in diameter), which are responsible for most root carbon storage, play a significant role in plant ecosystem function; they transfer water and nutrients (Dannoura *et al.* 2008). However, the study of coarse root systems is lacking because of the difficulty of underground observation and sampling. Traditional methods have many disadvantages in a large number of experiments such as considerable damage and operational complexity (Pransiska *et al.* 2016). Thus, non-destructive testing (NDT) methods are becoming popular for examining root systems (Hirano *et al.* 2009), due to their high efficiency and overall reliability of the information produced (Lv *et al.* 2018). Among these techniques, ground penetrating radar (GPR) is based on the scattering of electromagnetic waves radiating from a transmitting antenna. The radar signals form a reflection hyperbola at interfaces with different dielectric constants. Furthermore, the hyperbolic diffraction parameters (include two-way time delay, amplitude areas, pixels

within the threshold range, mean pixel intensity, and reflector tally, *etc.*) are formed to locate the roots, evaluate the biomass, and draw the root configuration in the case of the difference of the electrical parameters between root and the surrounding soils (Hruska *et al.* 1999; Reubens *et al.* 2007).

Great achievements have been made in the field of root detection, such as root biomass detection and the automatic 3D reconstruction of roots. Hruška *et al.* (1999) first applied GPR for coarse root detection and mapping. The major interests of using GPR to detect coarse roots thus far include: 1) coarse roots mapping and 2) coarse roots biomass and diameter estimation. Barton and Montagu (2004) tested the ability of GPR with 500 MHz, 800 MHz, and 1 GHz antennas to detect tree roots and determine roots size by burying roots in a 32 m³ pit containing damp sand. The root diameters were predicted with a root mean squared error of 0.6 cm, which allows the detection and quantification of roots as small as 1 cm in diameter. Amato *et al.* (2008) tested the ability of two-dimensional (2-D) DC resistivity tomography to detect the spatial variability of roots and to quantify their biomass in a tree stand. This study provided a basis for developing quick nondestructive methods for detecting root distribution and quantifying root biomass. Zhu *et al.* (2014) established a feasible detection method to delineate the root distributions from the acquired 3D data by 3D GPR, and proposed some reasonable indexes for estimating root biomass (including the biomass of a single root and total biomass in the specific depth ranges) in field conditions. Liu *et al.* (2018) analyzed the relationship between the shape of the GPR signals and root orientation, and explored the equation of hyperbola signals reflected by roots. In sum, there are many factors (radar frequency, diameter of the root, dielectric constant) in the *in situ* identification and detection of roots. When these factors are controllable, the identification accuracy of root will be more accurate.

Previous work on the detection of coarse roots either focused on studying the effect of radar frequency on GPR radargrams or using 3D GPR to directly image coarse root systems. These studies indicate that *in situ* recognition of the root should be valued both in root detection and in 3-D architecture of coarse roots. The correct interpretation of GPR radargrams is the first step in root detection and mapping coarse roots. Because the spatial distribution of roots affects radar reflection imaging, the present study focused on the spatial distribution of roots and applying GPR for coarse root detection and quantification.

The emphasis of this paper is the detection of root orientation and *in situ* recognition of coarse roots. First, a mathematical model of GPR echo wave signals was developed. A forward model about coarse roots in different orientations was established, and a method of locating roots was proposed, which combined the hyperbolic symmetry algorithm with the Hough transform algorithm. Third, a controlled experiment was used to evaluate the feasibility and effectiveness of a simulation experiment based on GPR datasets. Finally, the proposed method was verified using simulation and in the field experimental GPR data sets. The effect of root orientation on GPR hyperbolic is discussed.

EXPERIMENTAL

Materials

The GPR was purchased from TreeRadar Inc. (Silver Spring, MD, USA), which consists of a field data manager and a 900 MHz radar antenna. The experiment site was provided by the Summer Palace in Beijing.

Methods

Simulation model and GPR hyperbolic mathematical model

As shown in Fig. 1, the root (assuming it is completely straight for a finite length) was settled in a spatial rectangular coordinate system (the length and depth of the model are 0.24 m and 0.21 m, respectively) with one point in space as the original point. Both the root and the radar are in the positive coordinate system of space in order to display and analyze data more intuitively. The radar always moves along the same scan line, while the root rotates around its central point, which can construct roots in different orientations. The root orientation can be described by two parameters in the coordinate system: the horizontal orientation angle α ($0^\circ < \alpha < 90^\circ$) and the vertical inclination angle β ($0^\circ < \beta < 45^\circ$), as shown in Fig. 1a. The vertical inclination was defined as the angle of the projection of the root onto the y-z plane and z-axis. The azimuth angle was defined as the acute angle between the projection of the buried root onto the ground plane (x-z plane) and the orientation of the scanning line of the GPR (Liu *et al.* 2018).

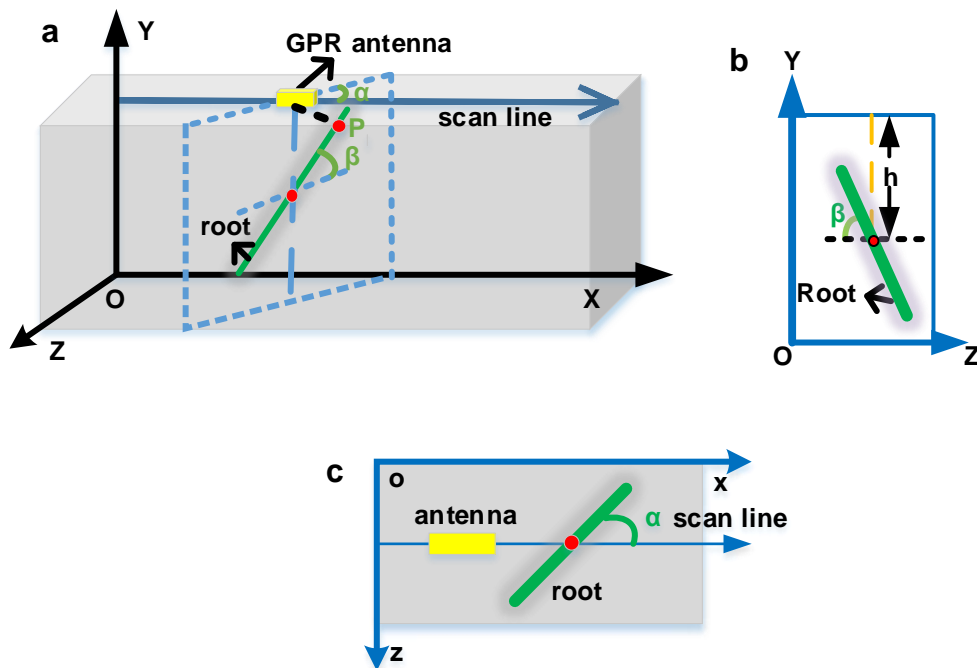


Fig. 1. Illustration of the simulation experiment scenario in spatial rectangular. (a) The whole figure of model; (b) the left view of model; and (c) the top view of model coordinate system.

When the GPR moved along the scan line, there is always a point P on a single root that is closest to the radar. In other words, the point P is always the spot where the earliest arrival of electromagnetic waves from radar as well as the reflected signal back to a radar receiver, t represented as a the “round-trip” travel time for a path that runs from the transmitter to the object then back to the receiver. Therefore, the GPR radargrams contain information of about the root orientation, and other information.

According to the theory of GPR, only when the roots extend horizontally or vertically to the crosscutting line of the scan line will it contain valid information about the signals (e.g., root diameter or biomass). Therefore, the curve formula for the roots in this case ($\alpha = 90^\circ$, $\beta = 0^\circ$) is needed. When the radar that sent and received electromagnetic

waves in parallel is close to the ground or almost close to the ground, it is assumed that the propagation path in the soil that is homogeneous medium becomes relatively simple, then the electromagnetic wave only was reflected back to the receiving antenna after hitting the target. The projection point of a target on a radar detection line is x_0 , as shown in Fig. 2 (Lee and Mokji 2015). In addition, the t_0 is a two-way travel time of x_0 , while z_0 and h (shown in Fig. 1b) are equivalent to the depth of a single root center in the ground. The center of the single root is P when $\beta = 0^\circ$. The β value affects the position of point P and the depth of the roots shown in the GPR radargrams. When GPR moves to x_i or x_0 , the electromagnetic waves emitted by the transmitter can reach the surface of the root with minimum distance. Therefore, according to the triangle Pythagorean theory, the hyperbola is represented by the following equation.

$$(z_i^2) - (x - x_0)^2 = (z_0)^2 \tag{1}$$

where, $z_0 = v \cdot t_0/2$ and $z_i = v \cdot t_i/2$, and z_i is the straight-line distance between GPR and P in the general position. The v denotes the velocity of the wave in homogeneous medium. It can be expressed as equation $= c/\sqrt{\epsilon_r}$, where c and ϵ_r are, respectively, indicated as the speed of light and the relative permittivity of GPR detected soil. Further, the formula (1) becomes:

$$\frac{(t_i)^2}{(t_0)^2} - \frac{(x-x_0)^2}{(v \cdot \frac{t_0}{2} + r)^2} = 1 \tag{2}$$

Equation 2 conforms to the constraint equation of a hyperbola ($\frac{x^2}{a^2} - \frac{y^2}{b^2} = 1$). However, the diameters of coarse roots cannot be ignored. At the same time, the GPR wave propagation path will change, as shown in Fig. 2b. Equation 1 becomes transformed into Eq. 3. Adding z_i and z_0 in Eq. 3 creates Eq. 4.

$$(z_i + r)^2 - (x - x_0)^2 = (z_0 + r)^2 \tag{3}$$

$$\frac{(t_i + \frac{2r}{v})^2}{(t_0 + \frac{2r}{v})^2} - \frac{(x-x_0)^2}{(v \cdot \frac{t_0}{2} + r)^2} = 1 \tag{4}$$

From these expressions, the information of a single root in the ground will be included in the GPR radargrams as a hyperbola ($a = t_0 + \frac{2r}{v}, b = v \cdot \frac{t_0}{2} + r$).

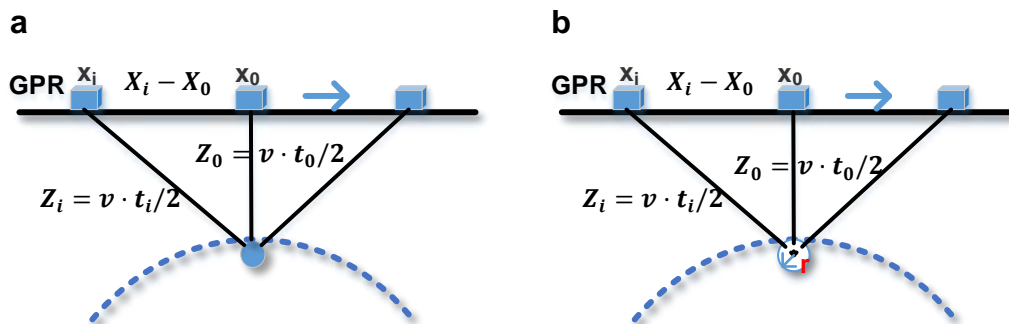


Fig. 2. The formation process of hyperbola when the single root has a diameter and is ideal. (a) The ideal situation ($r = 0$); and (b) the case of the existence of diameter ($r > 5$ mm)

However, the shape of the coarse root is not always an ideal cylinder, due to the ecological environment of trees. Only when the shape of the coarse root nears a cylinder can the GPR reflection image fit with the constraint equation of the standard hyperbola. On the other hand, the hyperbola also contains the information of electromagnetic wave velocity and dielectric constant of medium besides the parameters of the coarse root. Next, the characteristics of electromagnetic wave velocity in root reflection hyperbola will be described.

Symmetry algorithm and Hough transform algorithm

In this section, as shown in Fig. 3, a new algorithm was proposed that combined the symmetry algorithm with the Hough transform algorithm. The most prominent features of hyperbolic signals are the symmetry properties between the vertices and the monotonic decrease on both sides of the vertices, as shown in Fig. 2. The symmetry curve (indicated as Eq. 5) of the hyperbola is the most important step in the symmetry algorithm, and it was obtained by similar methods as Eriksson and Papanikotopoulos (1997) and Prasad and Yegnanarayana (2004).

$$S(j) = \sum_{i=1}^{y_{size}} \sum_{m=1}^k |f[i, j - m] - f[i, j + m]| \quad (5)$$

In Eq. 5, $j \in [k+1, y_{size}-k]$. In addition, the k is usually 0.2 or 1 of the effective caliber. The $f[i, j]$ is pixels of two-dimensional scan image obtained from GPR. The y_{size} and x_{size} are respectively the height and width of the image. The position corresponding to the minimum value of the symmetry curve $S[j]$ is the horizontal position corresponding to the hyperbolic vertex in the image.

The procedure for extracting the vertex of the GPR hyperbola is as follows:

- 1) Preprocessing: remove the direct wave, background noise, median filtering, and mean filtering by using Matgpr (Tzanis 2013).
- 2) Edge extraction, ROI generation and edge binary in a ROI: canny edge detection and extract the region of interests through adaptive threshold method. Finally, the ROI is binary.
- 3) Extract symmetry curve: judge the extreme points of the symmetry curve of GPR hyperbola, the number of extremum points is the same as the number of roots when the symmetry curves are not intersect, or otherwise; we need analyze if the intersection of the symmetry curve matches the characteristics of the roots or not. The minimum point of symmetry curve was obtained using Matlab (MathWorks, Natick, MA, USA) algorithm:

$$[m, n] = \min[S(j)] \quad (6)$$

where m is indicated as the scan number of hyperbola vertex, and the n is the minimum value of the symmetry curve.

- 4) Obtain the hyperbolic vertex delay: extract A-scan where the hyperbola vertex is located after extracting the horizontal position of hyperbola vertex. As shown in Fig. 4, the maximum amplitude point of the A-scan in the ROI is the time delay orientation coordinate (t) of the hyperbolic vertex.

To get the real depth of coarse roots, the electromagnetic wave velocity (v) of the medium is needed, as shown in Eq. 7.

$$h = v \cdot t/2 \quad (7)$$

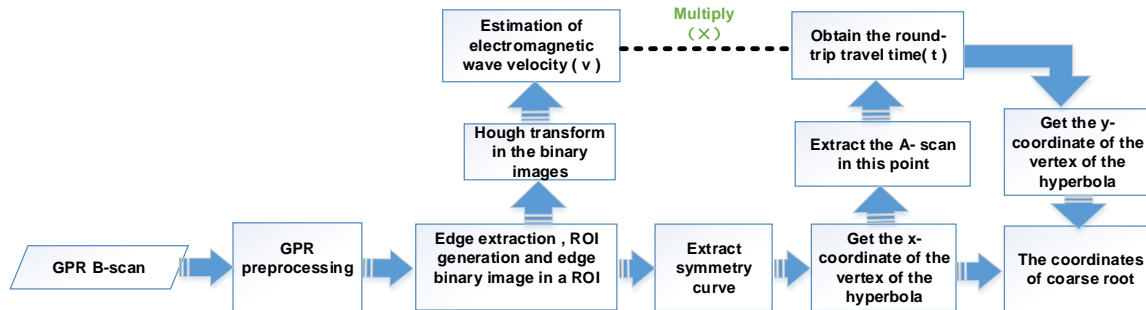


Fig. 3. The algorithm process chart, showing the combination of the two algorithms

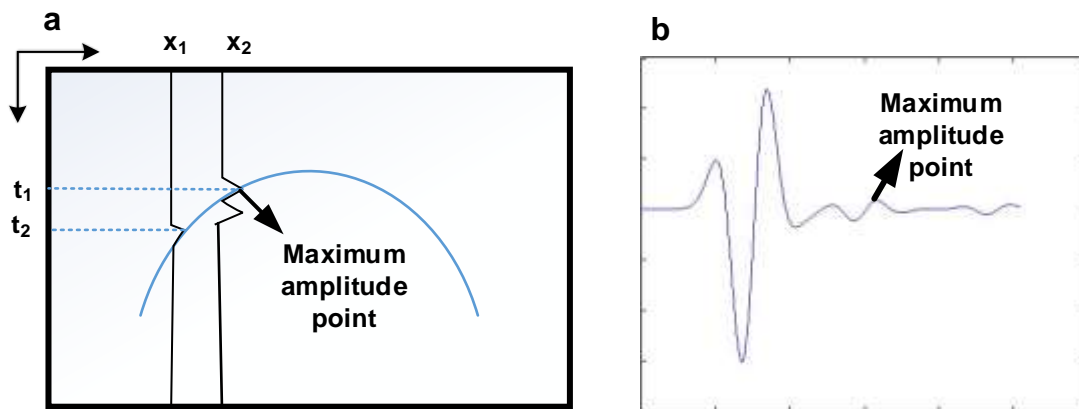


Fig. 4. Illustration of the maximum amplitude point. (a) Maximum amplitude point in the B-scan; (b) maximum amplitude point in the A-scan

In previous work, the hyperbolic curve was shown to contain information about the electromagnetic wave velocity (v), because the v is inversely proportional to the relative permittivity (affects the configuration of the hyperbola). At present, the methods to estimate wave velocity from GPR data mainly include Hough transform (Al-Nuaimy *et al.* 2000; Golovko 2004), curve fitting (Osumi and Ueno 1985; Al-Nuaimy *et al.* 2001; Zhu *et al.* 2005), and waveform offset in the frequency domain (Xu and Miller 2001). However, the latter two methods require a large amount of computation. The estimation accuracy depends on the trial step size, so it is not convenient to give the variance of the estimation. The effectiveness of wave velocity estimation is evaluated by known target depth test method and imaging effect method. Hough transform uses the principle of dot-line duality that the points of the common line in the image correspond to the intersecting lines in the parameter space. Similarly, all curves intersecting at the same point in the parameter space have collinear points corresponding to them in the GPR B-scan. According to the above analysis, the GPR B-scan is firstly converted to the parameter space depicted in Eqs. 8 and 9. The original equation (the illustration in Fig. 5a) of the hyperbola is shown in Eq. 8,

$$\left(\frac{v}{2} \times \Delta t \times y\right)^2 = [(x - x_0) \times \Delta x]^2 + \left(\frac{v}{2} \times \Delta t \times y_0\right)^2 \quad (8)$$

where v represents the speed of electromagnetic wave propagation in soil, Δt represents the time interval or sampling rate of GPR data collection, and Δx represents the move spacing (we set to 5 mm in general) of GPR. The x_0 is the x-coordinate of the vertex of the hyperbola, y_0 is the y-coordinate of the hyperbola. Equation 9 gives the final transform:

$$U = -K(x) \times V + x \quad (9)$$

where

$$V = \frac{1}{M} = \frac{(v \times \Delta t)^2}{4 \times \Delta x^2} \quad (10)$$

$$U = x_0 \quad (11)$$

$$K(x) = -y'(x) \times y(x) \quad (12)$$

In the above formulas, the hyperbolic equation has been converted to a linear parametric equation, as shown in Eqs. 9, 10, 11, and 12. Therefore after preprocessing and binary of hyperbola (shown in Fig. 5b), one $y'(x)$ is obtained as long as a point is taken on the binary image. Combined with $y(x)$, it is easier to get $K(x)$. At the same time, countless points $(-K(x), x)$ are obtained because the x is acquired. As a result, there is a line with a slope of $-K(x)$ and an intercept of x that in the V-U domain of the Hough transform, as shown in the Fig. 5c. Thus, the electromagnetic velocity v is calculated by Eq. 9 because v is contained in V , which is indicated as the intersection of many straight lines in the Hough coordinate system.

Subsequently, the h (the depth of coarse root or vertical coordinate of the coarse root position) was obtained in Eq. 7 based on the above conditions. The coordinate of single coarse root was known in the rectangular coordinate system (Fig. 1) as the x (the horizontal coordinate of the coarse root position) can be transformed from m (shown in Eqs. 6 and 15).

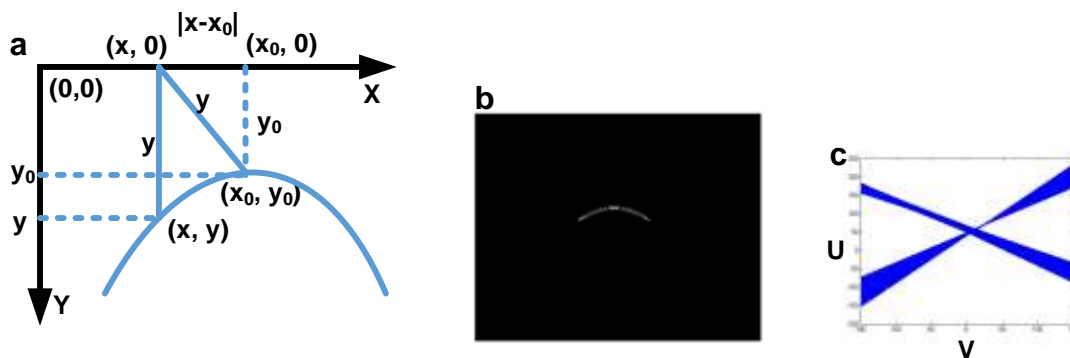








Fig. 5. (a) Mathematical form of the Hough Transformation of a hyperbola; (b) preprocessed in the original B-scan and edge extraction, ROI generation and edge binary in a ROI; (c) Hough Transform in the V-U domain

Simulation experiment, controlled experiment, and field experiment

In general, field experiments validate the feasibility of the algorithms that are used in the simulation experiments. Moreover, a simulation experiment is crucial in the whole inversion. The above models (shown in Fig. 1) were built with GprMax 3.0 software (University of Edinburgh, Dr. Antonis Giannopoulos, UK) based on Maxwell equations and the finite-different-time-domain theory (Giannopoulos 2005; Li *et al.* 2012). The root was 2 cm, and the waveform was a Ricker with an amplitude current of 1 A. For the convenience of radar detection, root depth was set to 10 cm. The scan number of GPR was set to 60. The time window was set to 3 ns, and the increment of each step of the antenna was 0.002 m. The dielectric constant permittivity of the soil and the root were 5 and 10, respectively. The dx , dy , and dz (PML boundary condition that can eliminate the noise caused by model boundary) were set to 0.002 m (Feng and Dai 2011). According to

previous research findings, the center frequency of the radar was set as 900 MHz, because this radar resolution is more suitable for shallow root detection (Hirano *et al.* 2009).

Table 1. Summary of Field Experiment in Summer Palace with Willow, Pine, and Cypress

Number	Species of Ancient Trees	Level of Ancient Trees	Edatope	Measuring Time	Location of Ancient Trees	Scene Picture
W1	willow	first-grade	fence ground pavement	2019.5.13	the north of Jiehu Bridge	
P1	pine	second-grade	ground pavement	2019.5.13	the south of North Palace Gate	
W2	willow	first-grade	fence ground pavement	2019.5.13	the south of Jiehu Bridge	
P2	pine	second-grade	slope dry soils	2019.5.14	the east of North Palace Gate	
C1	cypress	second-grade	grassland	2019.5.15	the west of Banbi Bridge	
C2	cypress	second-grade	grassland	2019.5.15	the east of Banbi Bridge	

In the simulation experiment, the root center was in the center of the model, and the root orientation was changed as it rotated around its center in a clockwise orientation. Based on the above factors, radar reflection images were obtained in different orientations of a single coarse root. These images can really well simulate the scene of different root orientations. Additionally, the simulated images were visualized by use of the imaging command in Matlab and underwent imagery preprocessing to enhance the image quality.

To verify the validity of simulation experiments, the controlled experiments in different root directions were carried out in the Gold Plant (40°29"N, 116°20'27" E). The region has a temperate continental monsoon climate with four distinct seasons. In the controlled experiment, grapevine was selected to simulate the detection of coarse roots. The surface of the study area is mainly fixed dune, and the soil type is mainly fine sand (Fig. 6a). The permittivity of natural fine sand is close to that of soil, and the physical properties are uniform. No rainfall occurred during the experiment, so the soil moisture content was stable and suitable for GPR detection.

In the controlled experiment, four roots with an average diameter of 2 cm were placed in a trench 2 m long and 1 m wide. The burial depth was 10 cm. The average water content of root was more than 30% because roots having high volumetric water content were easily detected (Guo *et al.* 2013). The soil dielectric constant was set to 5. To simulate roots with different vertical inclinations (Fig. 6a), the roots were obliquely inserted into the soil. Meanwhile, the radar scanned each root at different scanning angle (Fig. 6b). Finally, radar reflection images with different root directions were obtained in GPR radargrams.

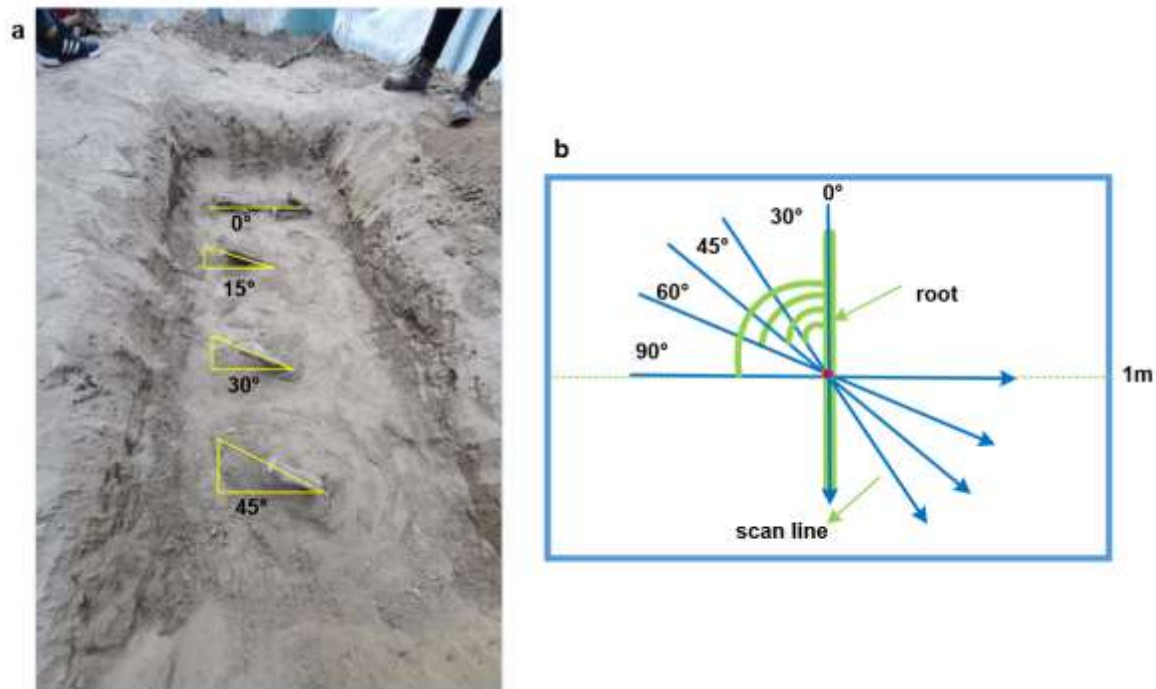


Fig. 6. (a) Field diagram of roots with different vertical inclinations ($\beta = 0^\circ, 15^\circ, 30^\circ, 45^\circ$); (b) the top view of schematic scene in different scanning angles of radar ($\alpha = 90^\circ, 60^\circ, 45^\circ, 30^\circ, 0^\circ$)

The field experiment was performed on the grounds of the Summer Palace ($39^\circ 59' 29''\text{N}$, $116^\circ 16' 19''\text{E}$). The Summer Palace, which is located in Haidian district of Beijing, has a temperate monsoon climate. The main vegetation in Park vegetation are cypress, pine, and willow; their roots are all coarse.

Table 1 shows the summary of the field experiment that contains test records for six trees. Two regions were selected for analysis: (1) the north of Banbi Bridge, and (2) the south of North Palace Gate (Fig. 7).

In general, the simulation experiment and controlled experiment can draw some correct conclusions. Distinguished by means of experiments under ideal conditions, there were many variables in the field. The pine and cypress trees were the main detection objects due to their difference in root growth. In the field, the orientation of the roots is uncertain because of the complexity of actual root growth. Nonetheless, the simulation experiment and controlled experiment can be used as prior knowledge to provide a basis for field experiments.



Fig. 7. The summary map of field experiment in Summer Palace: the display in Google map (especially two areas that located in the north of Banbi Bridge and the south of North Palace Gate)

RESULTS AND DISCUSSIONS

Effects of Root Orientation on the Reflecting Signal's Shape and *in situ* Identification

Figure 8b is the GPR B-scan after preprocessing of the image shown in Fig. 8a. Due to the negative reflectivity, the single root signal appears as the band of blue-red-blue contrary to soil echo signal.

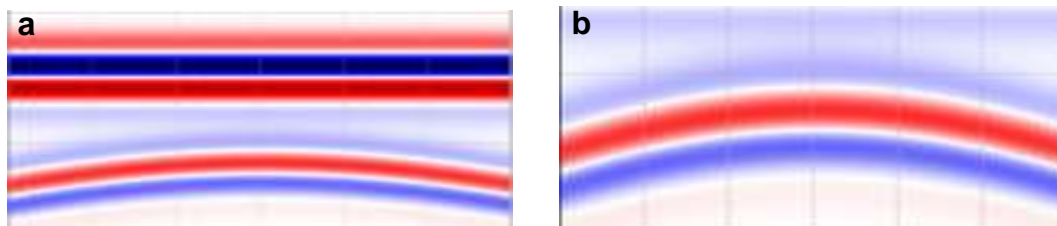


Fig. 8. (a) Original GPR B-scan; (b) GPR B-scan after preprocessing

In Supplementary Table 1, the alteration of the angle between the single coarse root and the GPR survey line led to the change in the shape of the B-scan. The horizontal angle

α and the vertical inclination β can influence, respectively, the shape of the hyperbola: 1) when $\beta=0^\circ$, the root of the hyperbola got flatter as α changed (from 90° to 0°); 2) if $\beta\neq 0^\circ$, as α diminished, the asymmetry of hyperbola appeared clearer; 3) the vertex of hyperbola would rise gradually when β increased (from 0° to 45°). Compared with the other orientation, the upper left corner of Supplementary Table 1 seemed to be the optimal case (the ideal state of simulation experiment).

The protrusive curve is the result from the inclination of single roots, which caused P to move up and narrowed the spacing between the GPR and the single root. As the GPR moved forward, the space of the scan step (Δx) was also affected by the change of inclination, which caused the different change rate of radar movement before and after point P, leading to the asymmetry of the curve.

Furthermore, the point P has two forms that, respectively, are P_0 in the model (the real P) and P_1 inversed by the algorithm. The coordinates of hyperbolae vertex (P_1) have been acquired by the proposed algorithm as shown in Table 4. On the other hand, there is a relationship between P_0 and O from a mathematical perspective (P_0 is collinear with O). From trigonometric function relation, the coordinate of P_0 can be expressed in the expression of the coordinates of O that include the inclination, and which are shown in the following equations:

$$\begin{aligned} X_0 &= x + (H - y) \times \sin \beta \times \cos \beta \times \cos \alpha \\ Y_0 &= (H - y) \times \sin 2\beta \end{aligned} \quad (13)$$

where x and y denote the horizontal and vertical coordinates of O, respectively, and H is the depth of GPR scanning. Finally, the relative error (RE; as shown in the upper right corner of Supplementary Table 2) was calculated from the following equations,

$$\begin{aligned} X_{RE} &= \frac{|X_1 - X_0|}{X_0} \times 100\% \\ Y_{RE} &= \frac{|Y_1 - Y_0|}{Y_0} \times 100\% \end{aligned} \quad (14)$$

where the quantities X_1 and Y_1 are obtained from the proposed algorithm as shown in the Table 4.

$$\begin{aligned} X_1 &= m \times \Delta x + d \\ Y_1 &= v \cdot t/2 \end{aligned} \quad (15)$$

where d denotes the initial position of the transmitting antenna, and v is defined by the Eqs. 9, 10, 11, and 12. The scanning number of hyperbola vertex (m) and time delay (t) was shown in Supplementary Table 2 (blue font).

To show the influence of inclination angle change on hyperbola more clearly, the symmetry curves of different orientations are shown in Supplementary Table 3. The symmetry algorithm directly reflects the degree of symmetry of hyperbola compared in the original B-scan. From the left to the right of the table, the symmetry point of the curve shifts to the right, and it becomes increasingly asymmetrical. In fact, the position of the symmetry point (the vertex of the hyperbola) is affected by both α and β , while the rise of the vertex was not shown in Supplementary Table 3. Nevertheless, it is worth noting that the symmetry curve is still a favorable representation of the symmetry of GPR hyperbola.

Table 4. Summary Figure (the finally inversion coordinate of P_1) of Simulated Data in Different Orientation of Single Coarse Root ($\alpha = 0^\circ, 15^\circ, 30^\circ, 45^\circ, 60^\circ, 75^\circ, 90^\circ$; $\beta = 0^\circ, 10^\circ, 15^\circ, 20^\circ, 30^\circ, 40^\circ, 45^\circ$)

$\alpha \backslash \beta$	0°	10°	15°	20°	30°	40°	45°
90°	(0.122, 0.0752)	(0.122, 0.0720)	(0.122, 0.0760)	(0.122, 0.0812)	(0.122, 0.0852)	(0.122, 0.0895)	(0.122, 0.0958)
75°	(0.122, 0.0759)	(0.122, 0.0758)	(0.126, 0.0791)	(0.128, 0.0824)	(0.128, 0.0864)	(0.130, 0.0898)	(0.130, 0.0962)
60°	(0.122, 0.0762)	(0.128, 0.0767)	(0.136, 0.0795)	(0.136, 0.0845)	(0.136, 0.0873)	(0.138, 0.0930)	(0.138, 0.0969)
45°	(0.122, 0.0760)	(0.152, 0.0767)	(0.148, 0.0805)	(0.146, 0.0850)	(0.146, 0.0886)	(0.146, 0.0938)	(0.146, 0.0978)
30°	(0.122, 0.0757)	(0.154, 0.0768)	(0.148, 0.0808)	(0.148, 0.0850)	(0.148, 0.0886)	(0.148, 0.0938)	(0.148, 0.0980)
15°	(0.122, 0.0756)	(0.154, 0.0772)	(0.150, 0.0808)	(0.152, 0.0848)	(0.152, 0.0888)	(0.152, 0.0952)	(0.152, 0.0978)
0°	(0.122, 0.0756)	(0.156, 0.0764)	(0.154, 0.0772)	(0.154, 0.0810)	(0.156, 0.0888)	(0.156, 0.0950)	(0.154, 0.0982)

Several studies have pointed out that in practice, the vertex of the hyperbola can have a dramatic impact on root detection. The movement of a vertex indirectly contains information about the direction of the coarse root. Therefore, the information regarding the coarse root orientation and inclination is incorporated in the characteristic hyperbolic shape. Curve fitting can be performed on the simulated data to generate more information about the coarse root.

To recognize coarse roots *in situ*, a simple and typical algorithm that combined Hough transform with symmetry algorithm was used. However, the reflection hyperbola of the root contains a lot of information, and the proposed algorithm has high computational cost. This algorithm can be improved in the future by using the random Hough transform to automatically recognize the hyperbola.

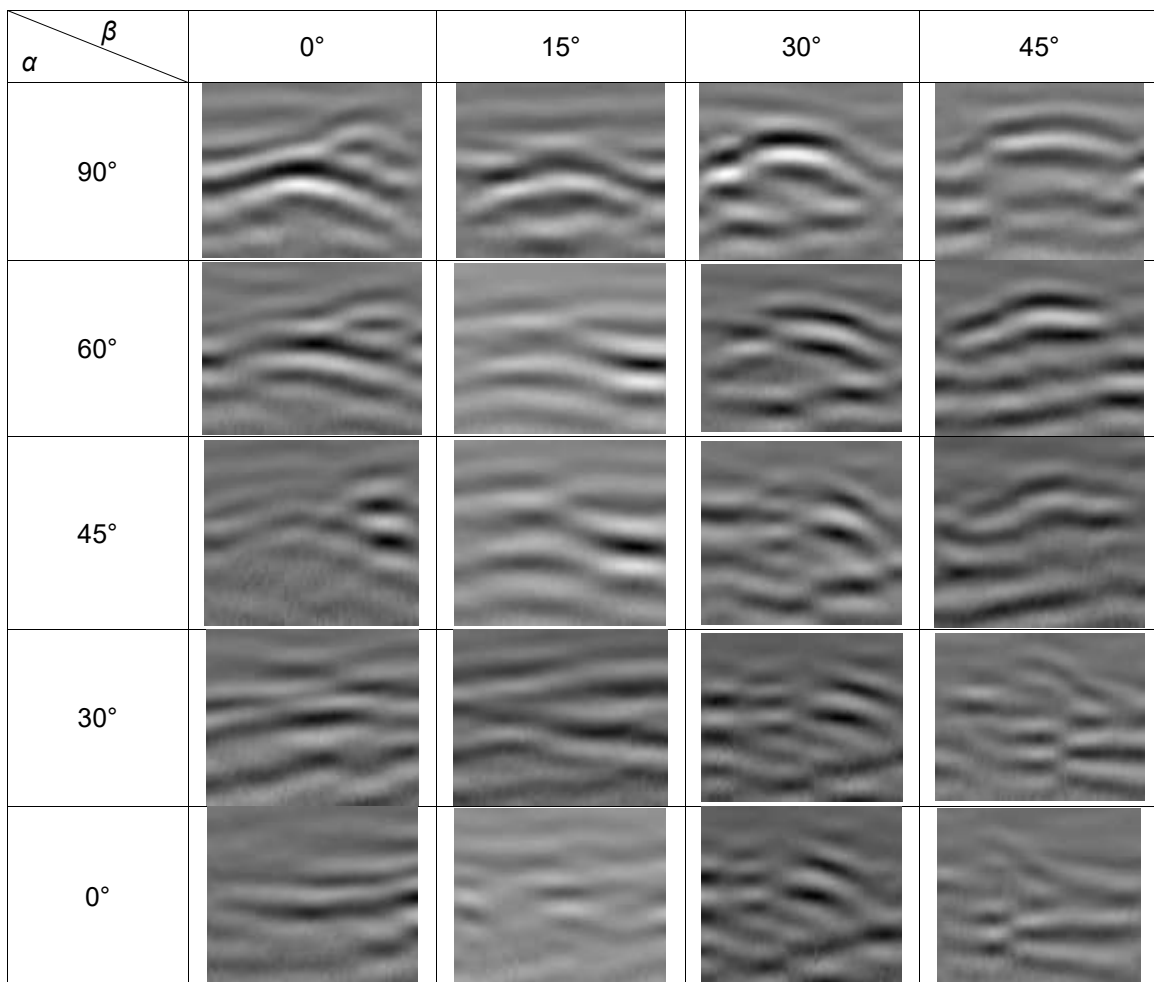
Overall, the results showed that the positions of the hyperbolic vertex move according to the change of the angle between the single root and the GPR survey lines. To some extent, the signal of root reflection hyperbola was discerned, although the *in situ* recognition of root was affected by a number of factors.

Effects of Root Orientation on Controlled Experiment

Table 5 shows radar reflection images after preprocessing in the controlled experiment. Previous studies have quantitatively evaluated the influence of root orientation on two major waveform parameters: amplitude area (A , dB ns) and time interval between zero crossings (T , ns). They clarified that the root reflection hyperbola was difficult to identify when the horizontal angle was $< 45^\circ$ (Guo *et al.* 2015; Tanikawa *et al.* 2013).

Similarly, in Table 5, there was no obvious hyperbola when $\alpha < 45^\circ$. Yet, in Supplementary Table 1, there were obvious hyperbola in GPR radargrams when $\alpha < 45^\circ$. As the simulation experiment was carried out under ideal conditions, the controlled experiment could not reach the same effect (Guo *et al.* 2012). Previous studies focused on the effect of horizontal inclination (α) on reflection hyperbola. Once β was taken into account in the control experiment, some patterns emerged: when $\alpha > 45^\circ$, 1) when $\beta=0^\circ$, the root of the hyperbola got flatter as α changed (from 90° to 45°), and the reflection intensity of the coarse root gradually became stronger; 2) if $\beta \neq 0^\circ$, as α became diminished, the asymmetry of hyperbolae appeared clearer; 3) the vertex of the hyperbola would rise gradually with increasing values of β (from 0° to 45°). Actually, in the controlled experiment, there were many background clutters in GPR radargrams due to the complexity of soil. This would affect the accuracy of coarse root recognition to some extent. Even so, results can confirm the priority and feasibility of GprMax in detecting coarse root.

Table 5. Summary Figure (GPR B-scan through preprocessing) of Controlled Experiment in Different Orientation of Single Coarse Root ($\alpha = 0^\circ, 30^\circ, 45^\circ, 60^\circ, 90^\circ$; $\beta = 0^\circ, 15^\circ, 30^\circ, 45^\circ$)



Effects of the Proposed Algorithm on Field Experiment

To obtain the optimal depth for GPR detection, the proposed algorithm was sent to the field radargrams. As shown in Fig. 9, four detection circles were set up, which indicated the GPR going around the tree in the specified radius, and the circle radii were 0.3 m, 0.45 m, 0.6 m, and 0.75 m. The signal curve presents a hyperbolic shape in the case of objects with different dielectric constants underground. Of course, there is no root if there are no hyperbola in GPR radargrams. As shown in Fig. 9, the outline of the hyperbola is represented by green dots (includes the vertex of hyperbola), and the red box indicates the presence of the hyperbola. Thus, the depth of 0.6 m is the most ideal one. Hyperbolas are not always equivalent to the coarse roots because the underground is particularly complex, having lots of cracks, pipes, foreign matter, *etc.* The single root curve is marked with the red box that is the only approximate positions of roots. The results suggest that it is feasible to apply the algorithm in recognition of root signals in most of the cases.

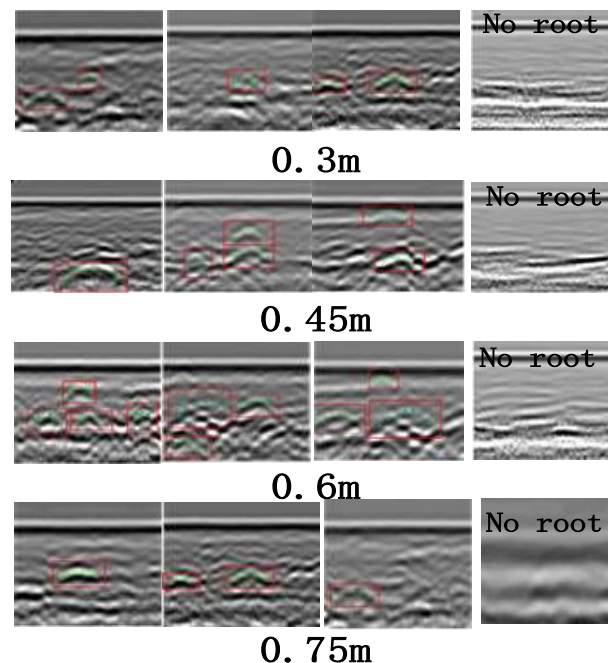


Fig. 9. The GPR reflection images of roots in the four detection circles, the radiuses respectively are 0.3 m, 0.45 m, 0.6 m, and 0.75 m (the red box is the hyperbola of the root, green dots represent feature points of root signal hyperbola).

Based on the aforementioned detection depth, two trees (one willow and one pine tree) were detected in the Summer Palace (Fig. 10). The root distribution (contains root diameter, root orientation) of the two trees is shown in eight detection circles (distances from the bark of 0.3 m, 0.6 m, 0.9 m, 1.2 m, 1.5 m, 1.8 m, 2.1 m, and 2.4 m). The different colored roots represent different depths of radar in the ground (red is 0 to 20 cm, green is 20 to 40 cm, and blue is 40 to 60 cm). The shallow roots (20 to 40 cm) predominate due to the appropriate water and nutrients, also is the main area of GPR detection. The roots of cypress trees are more concentrated than pine, whose roots are mainly on the southern side. The orientation of pine roots are more complex than cypress. However, these phenomena cannot be directly observed by the naked eye.

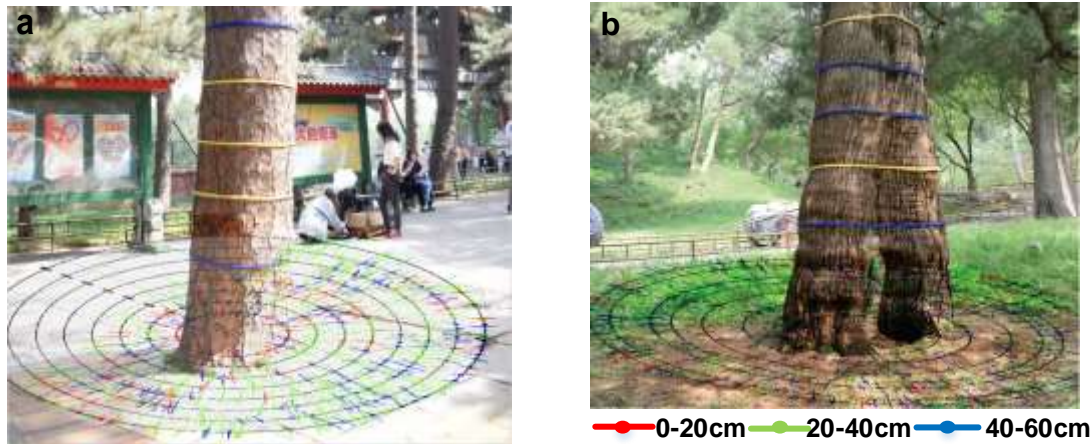


Fig. 10. Roots distribution (contains root diameter, root orientation) in the Summer Palace (the black wavy line points north, the red, green and blue lines represent different depths). (a): roots distributions (Contains eight detection circles) in the south of North Palace Gate; (b): roots distribution (Contains eight detection circles) in north of Banbi Bridge.

The distribution of the root systems was put into the three-dimensional tree to obtain the three-dimensional distribution of the root systems. According to an initial analysis of Fig. 10, the actual orientation of root systems was more complex. Thus, the reflecting hyperbola by GPR was more complex. Moreover, in-depth reconstruction of the roots' geometry was possible through a good deal of simulation experiments and field experiments.

CONCLUSIONS

1. The main goal of this paper was to analyze the reflected signals of coarse roots in different orientation, meanwhile, detecting and identifying coarse roots based on the simulation experiment. Through the comparison of simulation experiment and controlled experiment, the results suggest that the shape of the GPR hyperbola was affected by the root orientation, and the root reflection hyperbola was difficult to identify when $\alpha < 45^\circ$. Furthermore, the research about the influence of root direction on hyperbola formation is distinctly import.
2. However, there still exists many factors that affect the results of GPR detection and *in situ* recognition besides roots orientation, such as soil water content, root water content, root depth and interval, and center frequency of GPR. On the other hand, the proposed algorithm has the following limitations: (1) accuracy of recognition rate beyond the reach of the requirements in fine detection ($RE < 5\%$); (2) the high computational cost, and the robust performance is unsatisfied; (3) unable to implement automatic detection, and the results still require human intervention.
3. Though these factors restricted the detection of roots to some extent, our research still has significant science value. It is worth mentioning that the reason that the coarse roots were chosen for this experiment is because the coarse roots are easier to be detected than thin roots. The results can provide a theoretical basis and knowledge carrier for *in situ* identification of tree roots, as well as provide a theoretical study of root system biology, forestry, and underground ecology reconstruction of root systems.

ACKNOWLEDGMENTS

This research is financially supported by Beijing Natural Science Foundation (6202023) and the National Natural Science Foundations of China (Grant No. 31600589). Wenbin Li directed the research; Mingkai Wang and Jian Wen conceived and designed the experiments; Mingkai Wang implemented and performed the experiments; Mingkai Wang and Jian Wen analyzed and discussed the results. All authors wrote and revised the paper.

REFERENCES CITED

- Al-Nuaimy, W., Huang, Y., Eriksen, A., and Nguyen, V. T. (2001). "Automatic detection of hyperbolic signatures in ground-penetrating radar data," *Proceedings of SPIE - The International Society for Optical Engineering* 4491, 327-335.
- Al-Nuaimy, W., Huang, Y., Nakhkash, M., Fang, M. T. C., Nguyen, V. T., and Eriksen, A. (2000). "Automatic detection of buried utilities and solid objects with GPR using neural networks and pattern recognition," *Journal of Applied Geophysics* 43(2-4), 157-165. DOI: 10.1016/S0926-9851(99)00055-5
- Amato, M., Basso, B., Celano, G., Bitella, G., Morelli, G., and Rossi, R. (2008). "In situ detection of tree root distribution and biomass by multielectrode resistivity imaging," *Journal of Tree Physiology* 28(10), 1441-1448. DOI: 10.1093/treephys/28.10.1441
- Barton, C. V. M., and Montagu, K. D. (2004). "Detection of tree roots and determination of root diameters by ground penetrating radar under optimal conditions," *Journal of Tree Physiology* 24(12), 1323-1331. DOI: 10.1093/treephys/24.12.1323
- Dannoura, M., Hirano, Y., Igarashi, T., Ishii, M., Aono, K., Yamase, K., and Kanazawa, Y. (2008). "Detection of *Cryptomeria japonica* roots with ground penetrating radar," *Journal of Plant Biosystems* 142(2), 375-380. DOI: 10.1080/11263500802150951
- Eriksson, M., and Papanikotopoulos, N. P. (1997). "Eye-tracking for detection of driver fatigue," *Proceedings of Conference on Intelligent Transportation Systems*, Boston, MA, USA, DOI: 10.1109/ITSC.1997.660494
- Feng, D. S., and Dai, Q. W. (2011). "GPR numerical simulation of full wave field based on UPML boundary condition of ADI-FDTD," *NDT and E International* 44(6), 495-504. DOI: 10.1016/j.ndteint.2011.05.001
- Giannopoulos, A. (2005). "Modelling ground penetrating radar by GprMax," *J. Construction and Building Materials* 19(10), 755-762. DOI: 10.1016/j.conbuildmat.2005.06.007
- Golovko, M. M. (2004). "The automatic determination of soil permittivity using the response from a subsurface local object," *2004 Second International Workshop Ultrawideband and Ultrashort Impulse Signals*, Sevastopol, Ukraine. DOI: 10.1109/UWBUS.2004.1388117
- Guo, L., Cui, X., and Chen, J. (2012). "Sensitive factors analysis in using GPR for detecting plant roots based on forward modeling," *Progress in Geophysics* 4, 1754-1763.
- Guo, L., Lin, H., Fan, B., Cui, X., and Chen, J. (2013). "Impact of root water content on root biomass estimation using ground penetrating radar: evidence from forward simulations and field controlled experiments," *Journal of Plant and Soil* 371(1-2), 503-520. DOI: 10.1007/s11104-013-1710-4

- Guo, L., Wu, Y., Chen, J., Hirano, Y., Tanikawa, T., Li, W., and Cui, X. (2015). "Calibrating the impact of root orientation on root quantification using ground-penetrating radar," *Plant and Soil* 395(1-2), 289-305. DOI: 10.1007/s11104-015-2563-9
- Hirano, Y., Dannoura, M., Aono, K., Igarashi, T., Ishii, M., Yamase, K., Makita, N., and Kanazawa, Y. (2009). "Limiting factors in the detection of tree roots using ground-penetrating radar," *Journal of Plant and Soil* 319(1-2), 15-24. DOI: 10.1007/s11104-008-9845-4
- Hruska, J., Cermák J, and Sustek S. (1999). "Mapping tree root systems with ground-penetrating radar," *Journal of Tree Physiol.* 19(2), 125-130. DOI: 10.1093/treephys/19.2.125
- Lee, K. L., and Mokji, M. M. (2015). "Automatic target detection in GPR images using Histogram of Oriented Gradients (HOG)," *2014 2nd International Conference on Electronic Design (ICED)*, Penang, Malaysia. DOI: 10.1109/ICED.2014.7015795
- Liu, Q., Cui, X., Liu, X., Chen, J., Chen, X., and Cao, X. (2018). "Detection of root orientation using ground-penetrating radar," *IEEE Transactions on Geoscience and Remote Sensing* 56(1), 93-104. DOI: 10.1109/TGRS.2017.2737003
- Lv, G., Yang, J., Li, N., Hu, D., Zhang, Y., and Zhao, F. (2018). "Dielectric characteristics of unsaturated loess and the safety detection of the road subgrade based on GPR," *Journal of Sensors* 2018, 1-8. DOI: 10.1155/2018/5185460
- Osumi, N., and Ueno, K. (1985). "Microwave holographic imaging of underground objects," *IEEE Transactions on Antennas and Propagation* 33(2), 152-159. DOI: 10.1109/TAP.1985.1143559
- Ow, L. F., and Sim, E., K. (2012). "Detection of urban tree roots with the ground penetrating radar," *Plant Biosystems* 146(sup1), 10. DOI: 10.1080/11263504.2012.731018
- Pransiska, Y., Triadiati, T., Tjitrosoedirjo, S., Hertel, D., and Kotowska, M. M. (2016). "Forest conversion impacts on the fine and coarse root system, and soil organic matter in tropical lowlands of Sumatera (Indonesia)," *Journal of Forest Ecology and Management* 379, 288-298. DOI: 10.1016/j.foreco.2016.07.038
- Prasad, V. S. N., and Yegnanarayana, B. (2004). "Finding axes of symmetry from potential fields," *IEEE Transactions on Image Processing* 13(12), 1559-1566. DOI: 10.1109/TIP.2004.837564
- Reubens, B., Poesen, J., Danjon, F., Geudens, G., and Mays, B. (2007). "The role of fine and coarse roots in shallow slope stability and soil erosion control with a focus on root system architecture: A review," *Journal of Trees: Structure and Function* 21(4), 385-402. DOI: 10.1007/s00468-007-0132-4
- Tanikawa, T., Hirano, Y., Dannoura, M., Yamase, K., Aono, K., Ishii, M., Igarashi, T., Ikeno, H., and Kanazawa, Y. (2013). "Root orientation can affect detection accuracy of ground-penetrating radar," *Plant Soil* 373, 317-327. DOI: 10.1007/s11104-013-1798-6
- Tzani, A. (2013). "Detection and extraction of orientation-and-scale-dependent information from two-dimensional GPR data with tuneable orientational wavelet filters," *Journal of Applied Geophysics* 89, 48-67. DOI: 10.1016/j.jappgeo.2012.11.007
- Xu, X., and Miller, E. L. (2001). "Statistical method to localize buried landmines from GPR array measurement," *Proceedings of SPIE Volume 4394, Detection and*

- Remediation Technologies for Mines and Minelike Targets VI* - The International Society for Optical Engineering, Orlando, FL, USA. DOI: 10.1117/12.445527
- Zhu, Q., and Collins, L. M. (2005). "Application of feature extraction methods for landmine detection using the Wichmann/Niitek ground-penetrating radar," *IEEE Transactions on Geoscience and Remote Sensing* 43(1), 81-85.
DOI: 10.1109/TGRS.2004.839431
- Zhu, S., Huang, C., Su, Y., and Lu, M. (2014). "Tree roots detection based on circular survey using GPR," *Proceedings of the 15th International Conference on Ground Penetrating Radar*, Brussels, Belgium. DOI: 10.1109/ICGPR.2014.6970401
- Zhu, S., Huang, C., Su, Y., and Sato, M. (2014). "3D ground penetrating radar to detect tree roots and estimate root biomass in the field," *Journal of Remote Sensing* 6(6), 5754-5773. DOI: 10.3390/rs6065754

Article submitted: October 20, 2019; Peer review completed: January 14, 2020; Revised version received: January 22, 2019; Accepted: January 31, 2020; Published: February 7, 2020.

DOI: 10.15376/biores.15.2.2237-2257

APPENDIX**Supplemental**

Table S1. Summary Figure (GPR B-scan) of Simulated Data in Different Orientation of Single Coarse Root ($\alpha = 0^\circ, 15^\circ, 30^\circ, 45^\circ, 60^\circ, 75^\circ, 90^\circ$; $\beta = 0^\circ, 10^\circ, 15^\circ, 20^\circ, 30^\circ, 40^\circ, 45^\circ$)

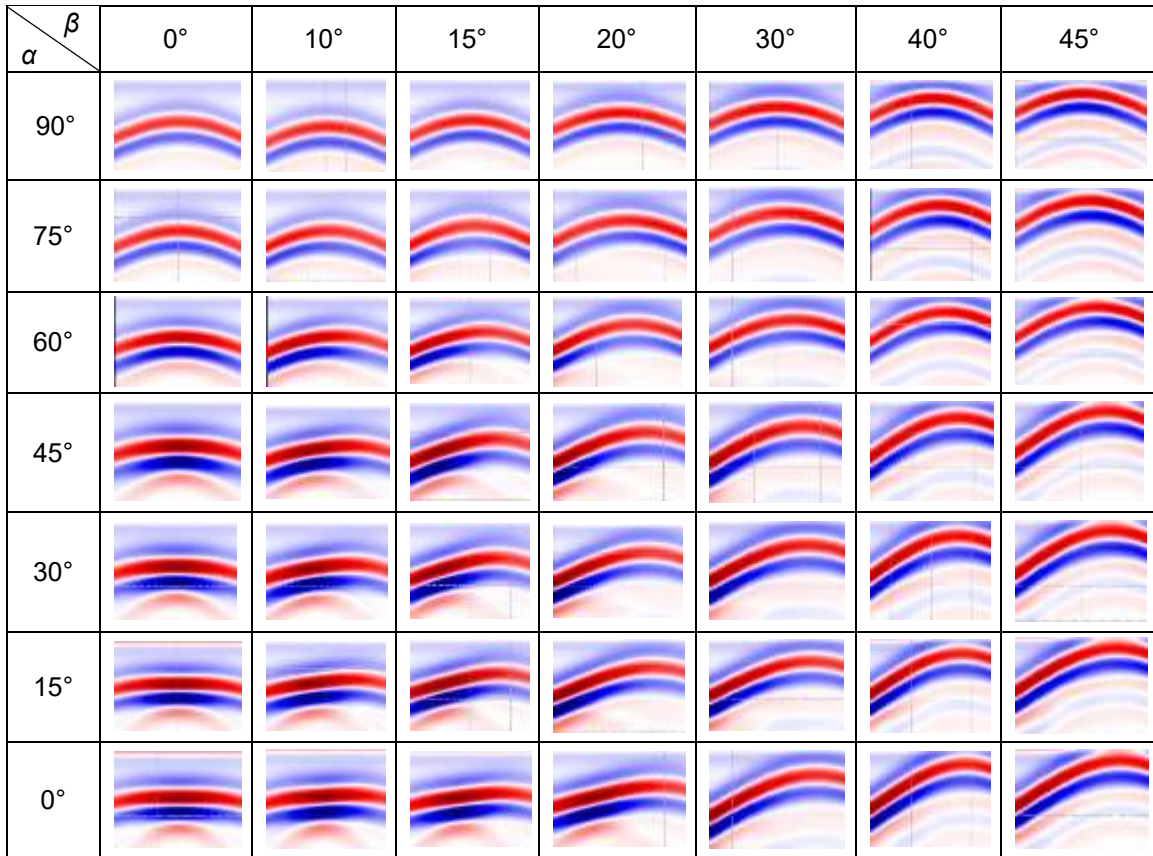


Table S2. Summary Figure (Initial Coordinate of P₁ and the Relative Error) of Simulated Data in Different Orientation of Single Coarse Root ($\alpha = 0^\circ, 15^\circ, 30^\circ, 45^\circ, 60^\circ, 75^\circ, 90^\circ; \beta = 0^\circ, 10^\circ, 15^\circ, 20^\circ, 30^\circ, 40^\circ, 45^\circ$)

$\alpha \backslash \beta$	0°	10°	15°	20°	30°	40°	45°
90°							
75°							
60°							
45°							
30°							
15°							
0°							

Table S3. Summary of Figures (Symmetry Curve of the Hyperbola of GPR) of Simulated Data in Different Orientation of Single Coarse Root ($\alpha = 0^\circ, 15^\circ, 30^\circ, 45^\circ, 60^\circ, 75^\circ, 90^\circ$; $\beta = 0^\circ, 10^\circ, 15^\circ, 20^\circ, 30^\circ, 40^\circ, 45^\circ$)

$\alpha \backslash \beta$	0°	10°	15°	20°	30°	40°	45°
90°							
75°							
60°							
45°							
30°							
15°							
0°							